Properties of 2 + 1-flavor QCD in the imaginary chemical potential region: A model approach

Junpei Sugano,[1,*] Hiroaki Kouno,[2,†] and Masanobu Yahiro[1,‡]

[1]*Department of Physics, Graduate School of Sciences, Kyushu University, Fukuoka 819-0395, Japan*
[2]*Department of Physics, Saga University, Saga 840-8502, Japan*

(Received 2 March 2017; published 27 July 2017)

We study properties of $2+1$-flavor QCD in the imaginary chemical potential region by using two approaches. One is a theoretical approach based on the QCD partition function, and the other is a qualitative one based on the Polyakov-loop extended Nambu–Jona-Lasinio (PNJL) model. In the theoretical approach, we clarify conditions imposed on the imaginary chemical potentials $\mu_f = i\theta_f T$ to realize the Roberge-Weiss (RW) periodicity. Here, T is the temperature, the index f denotes the flavor, and θ_f are dimensionless chemical potentials. We also show that the RW periodicity is broken if any one of θ_f is fixed to a constant value. In order to visualize the condition, we use the PNJL model as a model possessing the RW periodicity and draw the phase diagram as a function of $\theta_u = \theta_d \equiv \theta_l$ for two conditions of $\theta_s = \theta_l$ and $\theta_s = 0$. We also consider two cases, $(\mu_u, \mu_d, \mu_s) = (i\theta_u T, iC_1 T, 0)$ and $(\mu_u, \mu_d, \mu_s) = (iC_2 T, iC_2 T, i\theta_s T)$; here, C_1 and C_2 are dimensionless constants, whereas θ_u and θ_s are treated as variables. For some choice of C_1 (C_2), the number density of the up (strange) quark becomes smooth in the entire region of θ_u (θ_s) even in the high T region. This property may be important for lattice QCD simulations in the imaginary chemical potential region, since it makes the analytic continuation more feasible.

DOI: 10.1103/PhysRevD.96.014028

I. INTRODUCTION

One of the most important issues in hadron physics is to clarify the properties of quark matter in finite temperature and/or quark chemical potential. The knowledge of thermodynamics on quark matter is essential to understand the structure of the QCD phase diagram. As the review of the QCD phase diagram, see Refs. [1–4] and references therein.

Lattice QCD (LQCD) simulations may be the most promising and powerful theoretical tool of investigating the QCD phase diagram. As for isospin-symmetric two-flavor QCD, the fermion matrix is written as

$$\mathcal{M}(\mu_l) = \gamma_\mu D_\mu + m_l - \gamma_4 \mu_l \tag{1}$$

and satisfies γ_5 Hermiticity, $(\mathcal{M}(\mu_l))^\dagger = \gamma_5 \mathcal{M}(-\mu_l)\gamma_5$. Here, μ_l and m_l are the light-quark chemical potential and its mass, respectively. LQCD simulations are feasible for $\mu_l = 0$ since $\det \mathcal{M}(0)$ is real and positive definite. However, the fermion determinant becomes complex in finite μ_l because $(\det \mathcal{M}(\mu_l))^* = \det \mathcal{M}(-\mu_l) \neq \det \mathcal{M}(\mu_l)$ from the γ_5 Hermiticity. This is the well-known sign problem and makes the importance-sampling method unfeasible.

One of the ideas to circumvent the sign problem is the imaginary chemical potential $\mu_l = i\theta_l T$, where T is the temperature and θ_l is a dimensionless chemical potential. Indeed, the relation

$$(\mathcal{M}(i\theta_l T))^\dagger = \gamma_5 \mathcal{M}(i\theta_l T)\gamma_5 \tag{2}$$

can be obtained, and, hence, there is no sign problem, and positivity of the fermion determinant is also ensured. From the imaginary μ_l region, one can extract information of the real μ_l region by the analytic continuation. In fact, this approach was successful for the two-flavor QCD [5–14].

In the imaginary μ_l region, the QCD thermodynamic potential has the Roberge-Weiss (RW) periodicity [15], which can be regarded as a remnant of $\mathbb{Z}_3$ symmetry in the pure gauge limit. Also, in Ref. [15], it was shown that the first-order RW phase transition occurs at $\theta_l = (2k+1)\pi/3$ above some temperature $T_{\rm RW}$, where k is any integer; see Fig. 1. Because of the RW phase transition, information of the real μ_l region is limited up to $\mu_l/T \sim 1$, particularly at $T > T_{\rm RW}$.

As an alternative method of LQCD simulations, one can consider effective models. Among the effective models, the Polyakov-loop extended Nambu–Jona-Lasinio (PNJL) model is one of the most useful models and yields a good description of phenomena on quark matter, such as chiral and deconfinement transitions [16–28]. It was proven in Refs. [24–27] that the thermodynamic potential of the PNJL model possesses the RW periodicity for the two-flavor case, and the PNJL model reasonably reproduces LQCD data on the imaginary μ_l region [27,28].

In the case of $2+1$-flavor QCD, the strange-quark chemical potential μ_s is introduced as an additional external parameter, and the fermion determinant consists of the product $\det \mathcal{M}(\mu_l) \cdot \det \mathcal{M}(\mu_s)$. When both μ_l and μ_s are

*sugano@phys.kyushu-u.ac.jp
†kounoh@cc.saga-u.ac.jp
‡yahiro@phys.kyushu-u.ac.jp

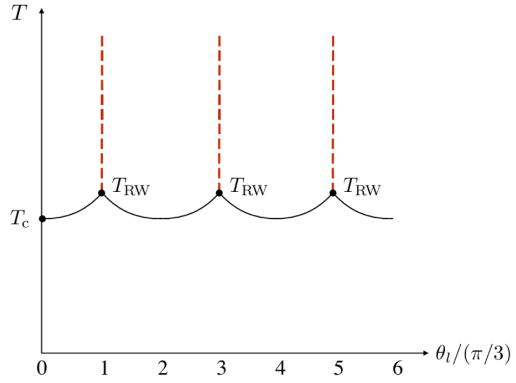

FIG. 1. Sketch of the phase diagram for the two-flavor QCD in the θ_l-T plane. The solid line is the crossover deconfinement transition line, and the vertical dashed line is the first-order RW phase transition line. The deconfinement transition temperature is represented by T_c. The label T_{RW} means the RW phase transition temperature.

pure imaginary, that is, when $\mu_l = i\theta_l T$ and $\mu_s = i\theta_s T$, the fermion determinant becomes real, and positivity of its determinant is guaranteed just as in the two-flavor case. Here, θ_s is a dimensionless chemical potential for the strange quark. It is, thus, suitable to consider the imaginary chemical potential region even in the $2+1$-flavor case, and some works were carried out [29–33]. In Ref. [30], the one-loop effective potential for the untraced Polyakov loop in the high T limit was calculated as a function of θ_l for two conditions, (I) $\theta_s = \theta_l$ and (II) $\theta_s = 0$, and they showed that the RW periodicity exists only in condition (I). In addition to this result, the calculation in the nonperturbative region is also necessary to acquire a better understanding of the RW phase transition.

Also, in Ref. [30], it was pointed out that the θ_l region available for analytic continuation becomes broader in condition (II) than in (I). This fact indicates that the analytic region can be expanded by breaking the RW periodicity deliberately. It is, therefore, interesting to consider how largely the analytic region is expanded by breaking the RW periodicity.

In this paper, we study the properties of the $2+1$-flavor QCD in the imaginary chemical potential region by using two approaches. One is a theoretical approach based on the QCD partition function, and the other is a qualitative one based on the PNJL model. In the theoretical approach, we first prove that the thermodynamic potential of nondegenerate three-flavor QCD has the RW periodicity in general, but the periodicity is lost when any one of the chemical potentials is fixed to a constant value. Next, as for the $2+1$-flavor case, we prove that the thermodynamic potential of the PNJL model has the same properties of QCD on the RW periodicity. For this reason, the PNJL model is used for qualitative analysis. We calculate some thermodynamic quantities and draw the phase diagram by using the PNJL model under conditions (I) and (II) in order to visualize the roles of the conditions. Finally, we evaluate the up- and strange-quark number densities for some choices of θ_l and θ_s. We numerically confirm that discontinuity of number densities due to the first-order phase transition disappears in the high T region, and the number densities become smooth. This property may be important for LQCD simulations in the imaginary chemical potential region, since it makes the analytic continuation more feasible even in high T region.

This paper is organized as follows: In Sec. II, we discuss the relation between the QCD thermodynamic potential and the RW periodicity. In Sec. III, the formalism of the PNJL model is explained, and the properties of the model in the imaginary chemical potential region are discussed. Section IV is devoted to the present numerical results calculated by the PNJL model. The summary is given in Sec. V.

II. QCD PARTITION FUNCTION AND RW PERIODICITY

Before going to the $2+1$-flavor case, we consider nondegenerate three-flavor QCD with imaginary μ_f ($f = u,\ d,\ s$). For later convenience, we introduce the dimensionless chemical potentials θ_f as $\mu_f = i\theta_f T$. In Euclidean spacetime with the time interval $\tau \in [0, \beta = 1/T]$, the QCD partition function $Z_{\rm QCD}$ is defined by

$$Z_{\rm QCD}(\theta_f) = \int \mathcal{D}A\mathcal{D}\bar{q}\mathcal{D}q \exp\left[-S_{\rm QCD}\right] \tag{3}$$

having the action

$$S_{\rm QCD} = \int d^4x \left[\bar{q}\left(\gamma_\mu D_\mu + \hat{m} - i\frac{\hat{\theta}}{\beta}\gamma_4\right)q + \frac{1}{4g^2}(F^a_{\mu\nu})^2\right], \tag{4}$$

where $q = (q_u, q_d, q_s)^{\rm T}$ is the quark field, $\hat{m} = {\rm diag}(m_u, m_d, m_s)$ is the current-quark mass matrix, and $D_\mu = \partial_\mu + iA_\mu$ is the covariant derivative including the gluon field $A_\mu = gA^a_\mu\lambda^a/2$ with the gauge coupling g and the Gell-Mann matrices λ^a. For the quark fields, the antiperiodic boundary conditions $q_f(\beta, \mathbf{x}) = -q_f(0, \mathbf{x})$ are imposed. The dimensionless chemical potential matrix $\hat{\theta}$ is defined by $\hat{\theta} = {\rm diag}(\theta_u, \theta_d, \theta_s)$.

We first redefine all the quark fields as

$$q_f \to \exp\left[i\frac{\theta_f}{\beta}\tau\right]q_f. \tag{5}$$

The integral measure is unchanged under Eq. (5), and $Z_{\rm QCD}$ is transformed into

$$Z_{\rm QCD}(\theta_f) = \int \mathcal{D}A\mathcal{D}\bar{q}\mathcal{D}q \exp\left[-S_{\rm QCD}\right],$$
$$S_{\rm QCD} = \int d^4x \left[\bar{q}(\gamma_\mu D_\mu + \hat{m})q + \frac{1}{4g^2}(F^a_{\mu\nu})^2\right] \quad (6)$$

with the boundary conditions

$$q_f(\beta, \mathbf{x}) = -e^{i\theta_f} q_f(0, \mathbf{x}). \quad (7)$$

Now, we consider $\mathbb{Z}_3$ transformation defined by

$$q_f \to U_k q_f, \quad (8)$$

$$A_\mu \to U_k A_\mu U_k^{-1} + i(\partial_\mu U_k)U_k^{-1}, \quad (9)$$

$$U_k = \exp\left[i\frac{2\pi k}{3}\frac{\tau}{\beta}\right], \qquad k \in \mathbb{Z}. \quad (10)$$

The functional form of $Z_{\rm QCD}$ keeps the form of Eq. (6) under the $\mathbb{Z}_3$ transformation, but the boundary conditions are changed into

$$q_f(\beta, \mathbf{x}) = -\exp\left[i\left(\theta_f - \frac{2\pi k}{3}\right)\right] q_f(0, \mathbf{x}). \quad (11)$$

Equations (6), (7), and (11) give the equality

$$Z_{\rm QCD}(\theta_f - 2\pi k/3) = Z_{\rm QCD}(\theta_f). \quad (12)$$

The QCD partition function, thus, has the periodicity of $2\pi/3$ in θ_f, which is nothing but the RW periodicity.

The RW periodicity of $Z_{\rm QCD}$ can be interpreted as the invariance under the extended $\mathbb{Z}_3$ transformation [24–27] composed of the shift $\theta_f \to \theta_f + 2\pi k/3$ and Eqs. (8)–(10). The QCD thermodynamic potential $\Omega_{\rm QCD}$ (per unit volume) is related with $Z_{\rm QCD}$ as $\Omega_{\rm QCD} = -T \ln Z_{\rm QCD}$. Therefore, $\Omega_{\rm QCD}$ also has the RW periodicity when $Z_{\rm QCD}$ is invariant under the extended $\mathbb{Z}_3$ transformation.

The discussions mentioned above can be applied to the 2 + 1-flavor case by setting $\theta_u = \theta_d \equiv \theta_l$. Hence, one can find that $\Omega_{\rm QCD}$ with condition (I) has the RW periodicity because of its invariance under the extended $\mathbb{Z}_3$ transformation. Meanwhile, when any one of θ_f is fixed to a constant value, for example, $\theta_s = 0$ in condition (II), the RW periodicity disappears since one cannot make the shift $\theta_f \to \theta_f + 2\pi k/3$ for fixed θ_f. This is the reason why the RW periodicity does not exist for condition (II). In the next section, we formulate the 2 + 1-flavor PNJL model and show that the PNJL model also possesses the same properties discussed in this section.

III. PNJL MODEL

The Lagrangian of the PNJL model in Euclidean spacetime is formulated by

$$\mathcal{L}_{\rm PNJL} = \bar{q}\left(\gamma_\mu D_\mu + \hat{m} - i\frac{\hat{\theta}}{\beta}\gamma_4\right)q + \mathcal{U}$$
$$- G_{\rm s}\sum_{a=0}^{8}[(\bar{q}\lambda^a q)^2 + (\bar{q}i\gamma^5\lambda^a q)^2]$$
$$+ K[\det{}_f\, \bar{q}(1+\gamma^5)q + \det{}_f\, \bar{q}(1-\gamma^5)q], \quad (13)$$

where the definitions of q, $\hat{m}$, and $\hat{\theta}$ are the same as in Eq. (4), but the covariant derivative has the form $D_\mu = \partial_\mu + ig\delta_{\mu 4}A^a_\mu\lambda^a/2$ in the present PNJL model. The Polyakov-loop potential $\mathcal{U}$ is a function of the Polyakov loop Φ and its conjugate Φ^*. The definitions of these quantities are

$$\Phi = \frac{1}{3}{\rm Tr}_{\rm c}(L), \qquad \Phi^* = \frac{1}{3}{\rm Tr}_{\rm c}(L^\dagger), \quad (14)$$

where $L = \exp[i\beta A_4] = \exp[i\beta{\rm diag}(A_4^{11}, A_4^{22}, A_4^{33})]$ for the classical gauge fields A_4^{ii} satisfying $A_4^{11} + A_4^{22} + A_4^{33} = 0$, and the trace is taken in color space. We use the logarithm type of

$$\mathcal{U} = T^4\left[-\frac{a(T)}{2}\Phi\Phi^* + b(T)\ln H\right], \quad (15)$$

$$a(T) = a_0 + a_1\left(\frac{T_0}{T}\right) + a_2\left(\frac{T_0}{T}\right)^2, \qquad b(T) = b_3\left(\frac{T_0}{T}\right)^3, \quad (16)$$

$$H = 1 - 6\Phi\Phi^* + 4(\Phi^3 + \Phi^{*3}) - 3(\Phi\Phi^*)^2 \quad (17)$$

in Ref. [22]. Note that Eq. (15) preserves the $\mathbb{Z}_3$ symmetry.

The original value of T_0 is fitted to 270 MeV so as to reproduce the deconfinement transition temperature in the pure gauge limit [34,35]. When the dynamical quarks are taken into account, the value of $T_0 = 270$ MeV predicts a higher deconfinement transition temperature than LQCD prediction, $T_{\rm c} \sim 160$ MeV at $\theta_f = 0$ [36–40]. The calculation in Ref. [41] provides lower $T_{\rm c}$ at $\theta_f = 0$ by refitting T_0 to a lower value, but we keep the original value to concentrate on qualitative discussions.

In the quark-quark interaction terms, $G_{\rm s}$ is the strength of the scalar-type four-point interaction, and K is the strength of the Kobayashi-Maskawa–'t Hooft (KMT) interaction [42–44]. The determinant in the KMT interaction term is taken in flavor space. The KMT interaction explicitly breaks $\mathrm{U_A}(1)$ symmetry and is necessary to reproduce the measured mass of η' meson at vacuum.

The mean-field approximation yields the thermodynamic potential $\Omega_{\rm PNJL}$ (per unit volume) as

$$\Omega_{\rm PNJL} = 2G_{\rm s}\sum_{f=u,d,s}\sigma_f^2 - 4K\sigma_u\sigma_d\sigma_s + \mathcal{U} - \frac{2}{\beta}\sum_{f=u,d,s}\int\frac{d^3\mathbf{p}}{(2\pi)^3}[3\beta E_f + \ln(1 + 3\Phi e^{-\beta(E_f-\mu_f)} + 3\Phi^* e^{-2\beta(E_f-\mu_f)} + e^{-3\beta(E_f-\mu_f)}) + \ln(1 + 3\Phi^* e^{-\beta(E_f+\mu_f)} + 3\Phi e^{-2\beta(E_f+\mu_f)} + e^{-3\beta(E_f+\mu_f)})], \quad (18)$$

where $\mu_f = i\theta_f T$, $\sigma_f = \langle\bar{q}_f q_f\rangle$, and $E_f = \sqrt{\mathbf{p}^2 + M_f^2}$ with the constituent-quark masses

$$M_f = m_f - 4G_{\rm s}\sigma_f + 2K\sigma_{f'}\sigma_{f''}, \quad (f \neq f', f' \neq f'', f \neq f''). \quad (19)$$

Note that $\theta_u = \theta_d \equiv \theta_l$, $\sigma_u = \sigma_d$, and $E_u = E_d$ in the $2+1$-flavor case. We introduce the three-dimensional cutoff Λ to regularize the vacuum term in Eq. (18). The variables $X = \{\sigma_l, \sigma_s, \Phi, \Phi^*\}$ are determined by the stationary conditions,

$$\frac{\partial\Omega_{\rm PNJL}}{\partial X} = 0, \qquad X = \{\sigma_l, \sigma_s, \Phi, \Phi^*\}. \quad (20)$$

The parameters used in the present PNJL model are summarized in Table I.

Under the extended $\mathbb{Z}_3$ transformation, the Polyakov loop behaves as $\Phi \to \Phi e^{-2\pi ik/3}$ and is not invariant. It is more convenient to define the flavor-dependent modified Polyakov loop and its conjugate [28] as

$$\Psi_f = e^{i\theta_f}\Phi, \qquad \Psi_f^* = e^{-i\theta_f}\Phi^*. \quad (21)$$

The extended $\mathbb{Z}_3$ transformation leaves these quantities invariant. After rewriting Eq. (18) by Ψ_f and Ψ_f^*, we can reach the expression

$$\Omega_{\rm PNJL} = 2G_{\rm s}\sum_{f=u,d,s}\sigma_f^2 - 4K\sigma_u\sigma_d\sigma_s + \mathcal{U} - \frac{2}{\beta}\sum_{f=u,d,s}\int\frac{d^3\mathbf{p}}{(2\pi)^3}[3\beta E_f + \ln(1 + 3\Psi_f e^{-\beta E_f} + 3\Psi_f^* e^{-2\beta E_f}e^{3i\theta_f} + e^{-3\beta E_f}e^{3i\theta_f}) + \ln(1 + 3\Psi_f^* e^{-\beta E_f} + 3\Psi_f e^{-2\beta E_f}e^{-3i\theta_f} + e^{-3\beta E_f}e^{-3i\theta_f})]. \quad (22)$$

The θ_f dependence of Eq. (22) is embedded in the extended $\mathbb{Z}_3$ symmetric quantities $\{e^{\pm 3i\theta_f}, \Psi_f, \Psi_f^*\}$. Obviously, $\Omega_{\rm PNJL}$ is invariant under the extended $\mathbb{Z}_3$ transformation, and, hence, $\Omega_{\rm PNJL}$ has the RW periodicity in general. Once any one of θ_f is fixed to some constant value, however, the extended $\mathbb{Z}_3$ transformation changes Ψ_f into $\Psi_f e^{-2\pi ik/3}$, and thereby $\Omega_{\rm PNJL}$ does not become invariant. It is, thus, concluded that $\Omega_{\rm PNJL}$ has the same properties as $\Omega_{\rm QCD}$ on the RW periodicity.

TABLE I. Summary of the parameter set used in the present PNJL model. The panels (a) and (b) are the parameter set in $\mathcal{U}$ [22] and the NJL part [45,46], respectively.

(a)	a_0	a_1	a_2	b_3	T_0 (MeV)
	3.51	−2.47	15.2	−1.75	270
(b)	m_l (MeV)	m_s (MeV)	Λ (MeV)	$G_{\rm s}\Lambda^2$	$K\Lambda^5$
	5.5	140.7	602.3	1.835	12.36

IV. NUMERICAL RESULTS

We show the numerical results calculated by the PNJL model. In the calculations of thermodynamic quantities and the QCD phase diagram, both conditions (I) and (II) are considered. We pick up $\Omega_{\rm PNJL}$ and the quark number density n_q as the thermodynamic quantities and calculate θ_l dependence for $T = 200$, 250 MeV. In the results of condition (I), the RW periodicity can be seen. On the contrary, there is no RW periodicity for condition (II), as expected in Sec. III. In the QCD phase diagram, we find for condition (II) that the crossover chiral transition line is discontinuous at some value of θ_l. In addition, the first-order phase transition line appears as is the RW phase transition line and can be fitted by a polynomial function of θ_l. Finally, the up- and strange-quark number densities are calculated under the situation that no RW periodicity exists. We show that the nonanalyticity in the number densities disappears below some constant value of θ_l or θ_s.

A. Behavior of thermodynamic quantities

The quark number density n_q is obtained by the relation

$$n_q = \sum_{f=u,d,s} n_f = i\beta \sum_{f=u,d,s} \frac{\partial}{\partial \theta_f} \Omega_{\mathrm{PNJL}}, \tag{23}$$

where n_f is the number density of the quark with flavor f. Using Eq. (23), we can see that n_q also has the RW periodicity when Ω_{PNJL} possesses the periodicity. Since Ω_{PNJL} is charge even, n_f is charge odd, namely, $\Omega_{\mathrm{PNJL}}(\theta_f) = \Omega_{\mathrm{PNJL}}(-\theta_f)$ and $n_q(-\theta_f) = -n_q(\theta_f)$.

Figure 2 presents Ω_{PNJL} and the imaginary part of n_q, $\mathrm{Im}(n_q)$, for condition (I), as a function of θ_l. The dotted line denotes the results for $T = 200$ MeV and the solid line does for $T = 250$ MeV. Both Ω_{PNJL} and n_q have the RW periodicity and are smooth for any θ_l when $T = 200$ MeV. Meanwhile, Ω_{PNJL} has cusps at $\theta_l = \pi/3 \bmod 2\pi/3$, and n_q becomes discontinuous there for $T = 250$ MeV. These singularities mean the first-order RW phase transition and indicate that the RW end point is located in $200 < T < 250$ MeV (see Fig. 4).

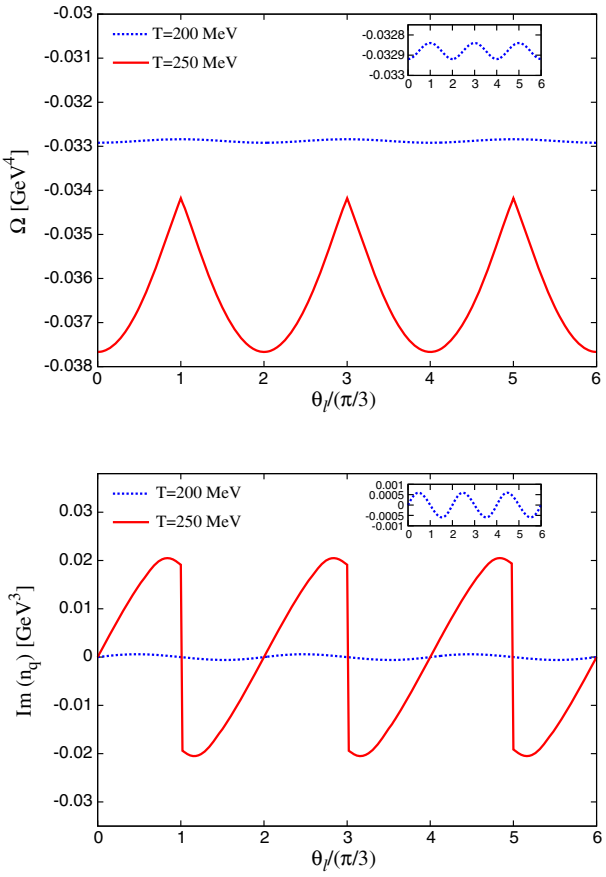

FIG. 2. The θ_l dependence of Ω_{PNJL} and the imaginary part of the quark number density $\mathrm{Im}(n_q)$ calculated by the PNJL model for condition (I). The solid line is the results for $T = 250$ MeV and the dotted line for $T = 200$ MeV.

Now, we concentrate on the region of $0 \le \theta_l \le 2\pi/3$. For charge-even quantities $\mathcal{O}_{\mathrm{even}}$ with the RW periodicity, such as Ω_{PNJL}, the relation

$$\begin{aligned}\mathcal{O}_{\mathrm{even}}(\theta_l - \epsilon) &= \mathcal{O}_{\mathrm{even}}(-\theta_l + \epsilon) \\ &= \mathcal{O}_{\mathrm{even}}(-\theta_l + 2\pi/3 + \epsilon)\end{aligned} \tag{24}$$

is obtained, where ϵ is a positive infinitesimal quantity. If the gradient

$$\lim_{\theta_l \to \pi/3 \pm 0} \frac{d\mathcal{O}_{\mathrm{even}}}{d\theta_l} \tag{25}$$

is neither zero nor infinity, charge-even quantities have a cusp at $\pi/3$. On the other hand, charge-odd quantities $\mathcal{O}_{\mathrm{odd}}$ possessing the RW periodicity, such as $\mathrm{Im}(n_q)$, satisfy

$$\begin{aligned}\mathcal{O}_{\mathrm{odd}}(\theta_l - \epsilon) &= -\mathcal{O}_{\mathrm{odd}}(-\theta_l + \epsilon) \\ &= -\mathcal{O}_{\mathrm{odd}}(-\theta_l + 2\pi/3 + \epsilon).\end{aligned} \tag{26}$$

Hence, discontinuity is seen at $\theta_l = \pi/3$ for charge-odd quantities in the high T region [24–26,47], where

$$\lim_{\theta_l \to \pi/3 \pm 0} \mathcal{O}_{\mathrm{odd}}(\theta_l) \neq 0. \tag{27}$$

Because of these singularities, the analytic continuation from the imaginary μ_l to the real one is limited up to $\theta_l = \pi/3$, particularly for the high T region.

Figure 3 is the same as Fig. 2 but for condition (II). It is clearly seen that the RW periodicity is lost, but θ_l dependence is similar between Figs. 2 and 3. In particular, the first-order phase transition still takes place for $T = 250$ MeV, and it is expected that its end point is located in $200 < T < 250$ MeV (see Fig. 5). We refer to this transition as the first-order "RW-like phase transition." It should be noted that the RW-like phase transition occurs at $\theta_l = 0.42\pi$ for $T = 250$ MeV. This result indicates that the region needed for the analytic continuation becomes broader for condition (II) than for (I), as already pointed out in Ref. [30].

B. Phase diagram

To determine the crossover chiral and deconfinement transition lines, we calculate the pseudocritical temperature of each transition by the peak position of susceptibilities for given θ_l. According to Ref. [48], the susceptibilities χ_{ij} of $\{\sigma_l, \sigma_s, \Phi, \Phi^*\}$ can be calculated by the inverse of dimensionless curvature matrix, $\chi_{ij} = (\mathcal{C}^{-1})_{ij}$, where

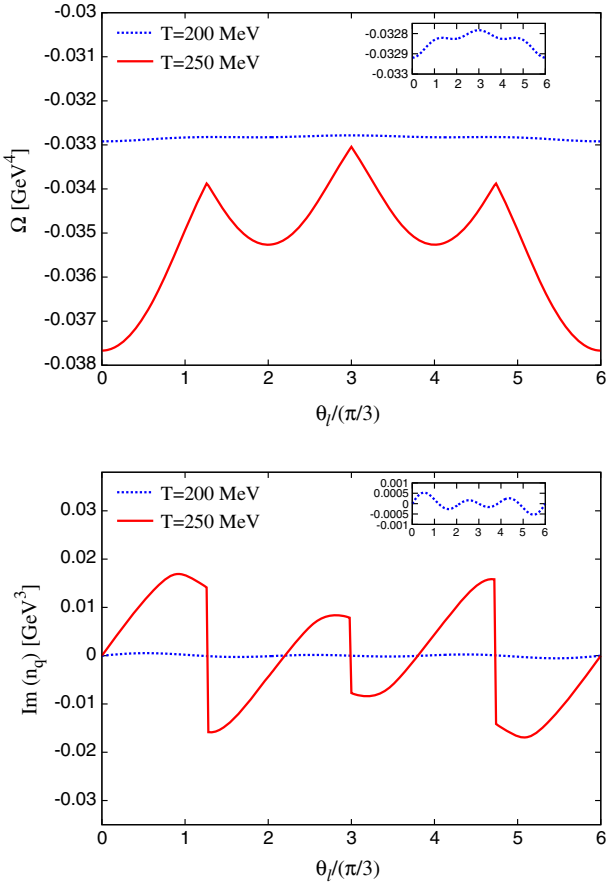

FIG. 3. The θ_l dependence of $\Omega_{\rm PNJL}$ and the imaginary part of the quark number density $\mathrm{Im}(n_q)$ calculated by the PNJL model for condition (II). The meanings of each line are the same as in Fig. 2.

$$\mathcal{C} = \begin{pmatrix} T^2 c_{\sigma_l\sigma_l} & T^2 c_{\sigma_l\sigma_s} & T^{-1} c_{\sigma_l\Phi} & T^{-1} c_{\sigma_l\Phi^*} \\ T^2 c_{\sigma_s\sigma_l} & T^2 c_{\sigma_s\sigma_s} & T^{-1} c_{\sigma_s\Phi} & T^{-1} c_{\sigma_s\Phi^*} \\ T^{-1} c_{\Phi\sigma_l} & T^{-1} c_{\Phi\sigma_s} & T^{-4} c_{\Phi\Phi} & T^{-4} c_{\Phi\Phi^*} \\ T^{-1} c_{\Phi^*\sigma_l} & T^{-1} c_{\Phi^*\sigma_s} & T^{-4} c_{\Phi^*\Phi} & T^{-4} c_{\Phi^*\Phi^*} \end{pmatrix} \tag{28}$$

with the abbreviation of

$$c_{xy} = \frac{\partial^2 \Omega_{\rm PNJL}}{\partial x \partial y}, \qquad x, y = \{\sigma_l, \sigma_s, \Phi, \Phi^*\}. \tag{29}$$

At the RW or RW-like phase transition points, n_q becomes discontinuous, as already shown in Figs. 2 and 3. This singular behavior is a good indicator to determine the location of the RW or RW-like phase transition points [47], and we use this property to determine the RW or RW-like phase transition lines. The usefulness of n_q to search the RW phase transition point is also discussed from the viewpoint of topological order [49].

Figure 4 presents the QCD phase diagram in the θ_l-T plane for condition (I). We only consider the region $\theta_l \in [0, 2\pi/3]$

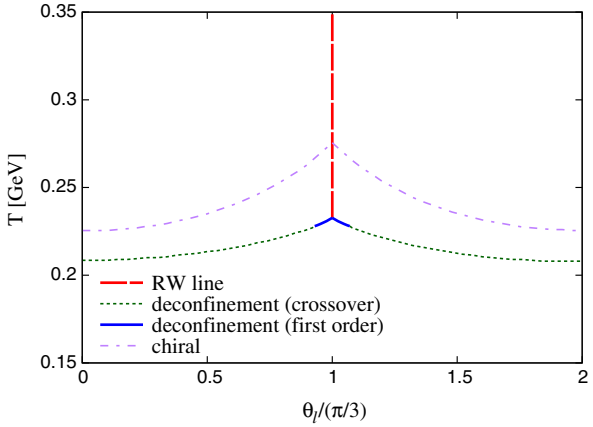

FIG. 4. The phase diagram in the θ_l-T plane for condition (I). The dashed line means the RW phase transition line. The crossover (first-order) deconfinement transition line is represented by the dotted (solid) line. The dot-dashed line corresponds to the crossover chiral transition line.

because of the RW periodicity. The dot-dashed line is the crossover chiral transition line, and the dotted line is the deconfinement one. The solid line denotes the first-order deconfinement transition line connected to the end point of the RW transition line represented by the dashed line. The RW end point is located at $(T^{\rm RW}, \theta_l^{\rm RW}) = (0.233\ \mathrm{GeV}, \pi/3)$. The chiral transition is crossover in the entire region, while the deconfinement transition becomes first order near the RW end point, which means that the RW end point is a triple point.

We comment on the order of the RW end point. The order of deconfinement transition depends on the Polyakov-loop potential $\mathcal{U}$ taken [28,47] and the entanglement coupling $G_s(\Phi, \bar{\Phi})$ [41,50,51]. For example, the deconfinement transition becomes second order [28,47] if we choose

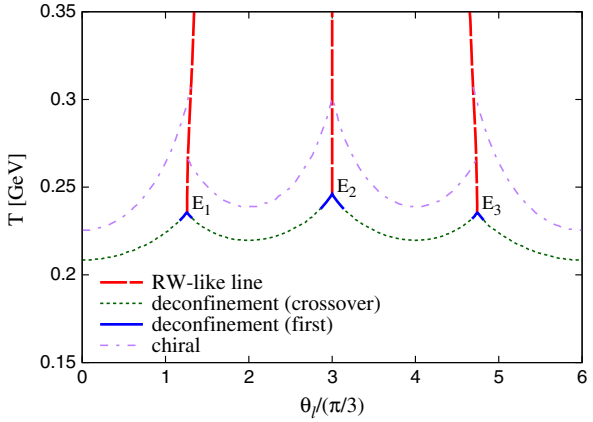

FIG. 5. The phase diagram in the θ_l-T plane for condition (II). The meanings of the lines are the same as in Fig. 4, except that the dashed line denotes the RW-like phase transition line. Each point of E_1, E_2, E_3 stands for the triple point of the RW-like phase transition line.

TABLE II. The location of points E_1, E_2, and E_3 in Fig. 5.

Point	E_1	E_2	E_3
(T, θ_l)	(0.236 GeV, 0.42π)	(0.246 GeV, π)	(0.236 GeV, 1.58π)

$$\mathcal{U} = -bT[54e^{-aT}\Phi\Phi^* + \log H] \tag{30}$$

as a form of $\mathcal{U}$ [18], where H is defined in Eq. (17) and a, b are parameters. In this case, the RW end point becomes a tricritical point. Also, in the PNJL model with the entanglement coupling

$$G_s(\Phi, \Phi^*) = G_s(1 - \alpha_1\Phi\Phi^* - \alpha_2(\Phi^3 + \Phi^{*3})) \tag{31}$$

and $(\alpha_1, \alpha_2) = (0.25, 0.1)$, the RW end point becomes a tricritical point [41]. This situation requires more robust studies to determine the order of the RW end point.

Figure 5 is the phase diagram for condition (II). The meaning of the lines is the same as in Fig. 4, except that the dashed line denotes the RW-like phase transition line. The location of points E_1, E_2, and E_3 is listed in Table II. The LQCD calculation of Ref. [30] predicts that the RW-like phase transition occurs at $\theta_l \cong 0.45\pi$ for $T = 208$ MeV. The PNJL model result $\theta_l = 0.42\pi$ for E_1 is consistent with the LQCD value $\theta_l \cong 0.45\pi$.

It is found that the RW periodicity is lost, but the phase diagram is line symmetrical with respect to $\theta_l = \pi$ because of the charge conjugation (C) symmetry of the PNJL model. The symmetry ensures that the chiral transition line has a cusp at point E_2. Meanwhile, the chiral transition line becomes discontinuous when it hits the RW-like line starting from points E_1 and E_3. As for the first-order deconfinement line, it becomes symmetric due to C symmetry around point E_2 but asymmetric around points E_1 and E_3.

In the region $\theta_l \in [0, 2\pi/3]$, the RW-like phase transition starts at E_1, i.e., $(T^{\mathrm{RW}'}, \theta_l^{\mathrm{RW}'}) = (0.236\ \mathrm{GeV}, 0.42\pi)$. We fit the transition line by the polynomial function

$$\theta_l(n_{\max}) = 0.42\pi + \sum_{n=1}^{n_{\max}} a_n\xi^n, \qquad \xi = \frac{T - T^{\mathrm{RW}'}}{T^{\mathrm{RW}'}}. \tag{32}$$

The transition line is well approximated by $\theta_l(n_{\max} = 3)$ with $a_1 = -0.023$, $a_2 = 0.93$, and $a_3 = -1.05$. The smallness of a_1 means that the line is nearly vertical in the vicinity of E_1 just as the RW phase transition line, but the transition line deviates from the vertical line as T increases.

The RW-like phase transition line also appears when we consider the imaginary isospin chemical potential $\mu_I = i\theta_I T$, where θ_I is a dimensionless isospin chemical potential. In the θ_I-T plane, the RW-like phase transition line is almost vertical and described by $\theta_I = \pi/2 - \delta(T)$ with [29]

$$\delta(T) = 0.00016 \times (T - 250). \tag{33}$$

For the details, see Refs. [28,29].

In Figs. 4 and 5, the deconfinement transition line joins the RW or RW-like end points, and the chiral transition line is higher than the deconfinement one. In the LQCD calculation of Ref. [32], however, the chiral transition line is connected to the end points. At the present stage, our model cannot explain the LQCD result. What happens at the end points? This is an interesting future work from the theoretical point of view.

Finally, we compare the chiral transition line $T = T_{\mathrm{chiral}}(\theta_l)$ calculated by the PNJL model with that by LQCD simulations of Ref. [31]; note that θ_l varies with θ_s fixed at either 0 or θ_l. The ratio $R = T_{\mathrm{chiral}}(\theta_l)/T_{\mathrm{chiral}}(0)$ is charge even and can be parametrized by [30,31]

$$R = 1 + 9\kappa\theta_l^2 + b\theta_l^4 \tag{34}$$

with the curvature κ of the transition line and some constant b, when θ_l is not large.

Figure 6 represents θ_l^2 dependence of R calculated from the PNJL model and LQCD simulations. The PNJL model well reproduces LQCD data for $\theta_s = \theta_l$ and is almost consistent with LQCD data for $\theta_s = 0$. Thus, the present PNJL model may be good enough for qualitative analyses.

C. Analyticity of number density

We calculate the imaginary part of the up- and strange-quark number densities $\mathrm{Im}(n_u)$ and $\mathrm{Im}(n_s)$ by using the PNJL model. We consider the situation that the RW periodicity does not exist; that is, some chemical potentials are fixed to constant values. Only in the calculations of $\mathrm{Im}(n_u)$ are θ_d and θ_s treated as constants. As for the calculations in the θ_s dependence of $\mathrm{Im}(n_s)$, we again

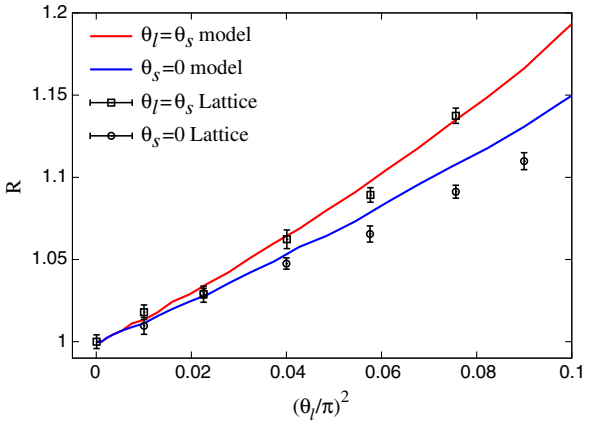

FIG. 6. θ_l^2 dependence of ratio $R = T_{\mathrm{chiral}}(\theta_l)/T_{\mathrm{chiral}}(0)$. The horizontal axis is normalized by π^2. The model calculations are represented by solid lines, and the data with error bars mean LQCD results [31].

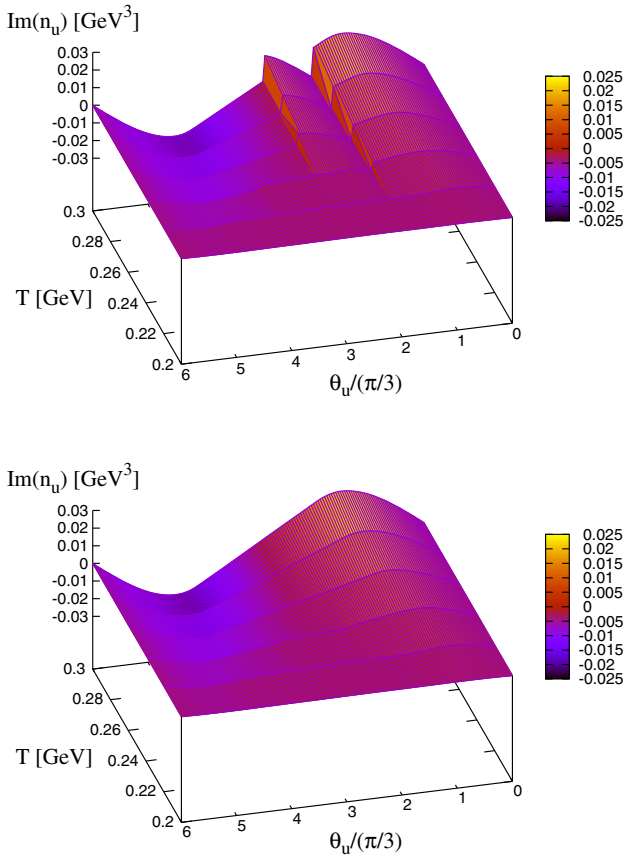

FIG. 7. The θ_u and T dependence of $\mathrm{Im}(n_u)$. The upper panel is the result with $(\theta_d, \theta_s) = (\pi/4, 0)$, and the lower panel is the one with $(\theta_d, \theta_s) = (\pi/8, 0)$.

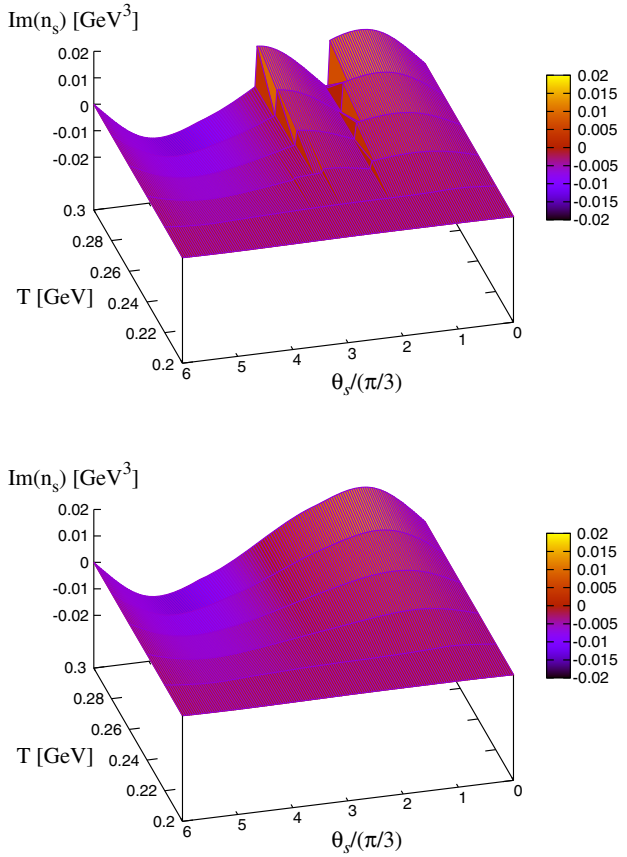

FIG. 8. The θ_s and T dependence of $\mathrm{Im}(n_s)$. The upper panel is the result with $\theta_l = \pi/4$, and the lower panel is the one with $\theta_l = \pi/5$.

consider $\theta_u = \theta_d = \theta_l$, and these are fixed to constant values.

Figure 7 shows the θ_u and T dependence of $\mathrm{Im}(n_u)$. The upper panel is the result for $(\theta_d, \theta_s) = (\pi/4, 0)$ and the lower one is for $(\theta_d, \theta_s) = (\pi/8, 0)$. In the upper panel, $\mathrm{Im}(n_u)$ becomes discontinuous because of the RW-like phase transition but smooth at any T in the lower panel. We numerically checked that $\mathrm{Im}(n_u)$ becomes smooth at any T when $\theta_s = 0$ and $\theta_l \leq \pi/8$.

Figure 8 is the result of $\mathrm{Im}(n_s)$ as a function of θ_s and T. The upper panel corresponds to the result for $\theta_l = \pi/4$, and the lower panel is the result for $\theta_l = \pi/5$. It is found that the discontinuity of $\mathrm{Im}(n_s)$ disappears for any T when $\theta_l = \pi/5$, while $\mathrm{Im}(n_s)$ becomes discontinuous when $\theta_l = \pi/4$ due to the RW-like phase transition. We also numerically confirmed that $\mathrm{Im}(n_s)$ has no discontinuity for any T when $\theta_l \leq \pi/5$. The results in Fig. 7 (Fig. 8) indicate that n_u (n_s) in the real μ_u (μ_s) region can be easily obtained by the analytic continuation from the entire imaginary region. The present case is, thus, more informative compared to the case where the RW periodicity exists.

The n_{s} in the high T region plays a key role in determining the strength of the repulsive interaction,

$$\mathcal{L}_{\mathrm{v,s}} = -G_{\mathrm{v,s}}(\bar{s}\gamma^{\mu}s)^2, \tag{35}$$

where s is the strange-quark field and $G_{\mathrm{v,s}}$ is its strength. The behavior of n_{s} is sensitive to the value of $G_{\mathrm{v,s}}$ because n_{s} is a function of

$$\tilde{\mu}_{\mathrm{s}} = \mu_{\mathrm{s}} - 2G_{\mathrm{v,s}}n_{\mathrm{s}} \tag{36}$$

after the mean-field approximation.

In our previous works [52], it was shown that the strength G_{v} of the vector-type four-quark interaction

$$\mathcal{L}_{\mathrm{v}} = -G_{\mathrm{v}}(\bar{q}\gamma^{\mu}q)^2 \tag{37}$$

can be determined from LQCD data on the quark number density n_q in the high T region [14,53]. We then pinned down the value of G_{v} from LQCD data on n_q. However, this analysis did not consider the strange quark. Figure 8 indicates that the analytic continuation from imaginary μ_s to real μ_s works well even in the high T region. Thus, one can get reliable n_{s} in both the real- and the imaginary-μ_s regions. This allows us to determine the value of $G_{\mathrm{v,s}}$ sharply from the LQCD data.

The interaction described by Eq. (35) corresponds to the interaction mediated by the ϕ meson in the context of the relativistic mean-field theory [54–58] and affects the maximum mass of a neutron star when the strange quark exists in the inner core of the neutron star. It is an interesting future work to investigate the interplay between the $G_{v,s}$ determined from the LQCD data and the maximum mass and to discuss what happens in the two-solar-mass neutron star [59,60].

V. SUMMARY

In this paper, we investigated properties of the $2+1$-flavor QCD in the imaginary chemical potential region with finite $\mu_l = i\theta_l T$ and $\mu_s = i\theta_s T$ using two approaches. One is a theoretical approach based on the QCD partition function and the other is a qualitative one based on an effective model. In the theoretical approach, we proved that the QCD thermodynamic potential $\Omega_{\rm QCD}$ exhibits the RW periodicity only when $\Omega_{\rm QCD}$ is invariant under the extended $\mathbb{Z}_3$ transformation. In other words, the RW periodicity disappears when two chemical potentials are fixed to a constant value. Next, we showed that the thermodynamic potential of the PNJL model also possesses the extended $\mathbb{Z}_3$ symmetry. We then took the PNJL model as a useful effective model.

Taking the PNJL model, we calculated $\Omega_{\rm PNJL}$, $\mathrm{Im}(n_q)$ (the imaginary part of quark number density), and the QCD phase diagram as a function of θ_l for two conditions: (I) $\theta_s = \theta_l$ and (II) $\theta_s = 0$. For condition (I), the RW periodicity is seen in all the results. The structure of the phase diagram is similar to the one in the two-flavor case [28]. As for condition (II), there is no RW periodicity, but we found that the region available for the analytic continuation is broader than condition (I). The noteworthy points on the phase diagram are the following:

(1) The crossover chiral transition line becomes discontinuous on the RW-like phase transition line.
(2) The first-order deconfinement transition line is asymmetric with respect to the RW-like phase transition line, except for at $\theta_l = \pi$.
(3) The first-order RW-like phase transition line can be well fitted by a polynomial function of Eq. (32) with $n_{\rm max} = 3$.

Finally, we calculated the imaginary part of the up- and strange-quark number densities, $\mathrm{Im}(n_u)$ and $\mathrm{Im}(n_s)$. We considered the situation that two chemical potentials are fixed to constant values, and thereby the RW periodicity disappears. When $\theta_s = 0$ and $\theta_d \le \pi/8$, $\mathrm{Im}(n_u)$ becomes an analytic function of θ_u for any T. The condition for $\mathrm{Im}(n_s)$ to be an analytic function of θ_s for any T is $\theta_u = \theta_d = \theta_l \le \pi/5$. When these conditions are satisfied, the values of n_u and n_s can be easily calculated by the analytic continuation, for any T of interest.

In the present paper, we concentrated on a qualitative discussion based on the extended $\mathbb{Z}_3$ symmetry. The results mentioned above are interesting theoretically but do not exactly correspond to the realistic case. As a future work, it is quite interesting to make systematic and quantitative analyses, particularly in more realistic cases.

ACKNOWLEDGMENTS

The authors thank K. Kashiwa, M. Ishii, and S. Togawa for useful discussions and comments. J. S., H. K., and M. Y. are supported by Grant-in-Aid Scientific Research (Grants No. 27-7804, No. 26400279, No. 17K05446, and No. 26400278) from the Japan Society for the Promotion of Science.

[1] M. Stephanov, arXiv:0701002.
[2] P. Braun-Munzinger and J. Wambach, Rev. Mod. Phys. **81**, 1031 (2009).
[3] K. Fukushima and T. Hatsuda, Rep. Prog. Phys. **74**, 014001 (2011).
[4] K. Fukushima and C. Sasaki, Prog. Part. Nucl. Phys. **72**, 99 (2013).
[5] P. de Forcrand and O. Philipsen, Nucl. Phys. **B642**, 290 (2002).
[6] M. D'Elia and M. P. Lombardo, Phys. Rev. D **67**, 014505 (2003).
[7] L. K. Wu, X. Q. Luo, and H. S. Chen, Phys. Rev. D **76**, 034505.
[8] M. D'Elia and F. Sanfilippo, Phys. Rev. D **80**, 111501 (2009).
[9] P. de Forcrand and O. Philipsen, Phys. Rev. Lett. **105**, 152001 (2010).
[10] K. Nagata and A. Nakamura, Phys. Rev. D **83**, 114507 (2011).
[11] P. Cea, L. Cosmai, M. D'Elia, A. Papa, and F. Sanfilippo, Phys. Rev. D **85**, 094512 (2012).
[12] J. Takahashi, K. Nagata, T. Saito, A. Nakamura, T. Sasaki, H. Kouno, and M. Yahiro, Phys. Rev. D **88**, 114504 (2013).
[13] C. Bonati, P. de Forcrand, M. D'Elia, O. Philipsen, and F. Sanfilippo, Phys. Rev. D **90**, 074030 (2014).
[14] J. Takahashi, H. Kouno, and M. Yahiro, Phys. Rev. D **91**, 014501 (2015).
[15] A. Roberge and N. Weiss, Nucl. Phys. **B275**, 734 (1986).
[16] P. N. Meisinger and M. C. Ogilvie, Phys. Lett. B **379**, 163 (1996).

[17] A. Dumitru and R. D. Pisarski, Phys. Rev. D **66**, 096003 (2002).
[18] K. Fukushima, Phys. Lett. B **591**, 277 (2004); Phys. Rev. D **77**, 114028 (2008); **78**, 114019 (2008).
[19] S. K. Ghosh, T. K. Mukherjee, M. G. Mustafa, and R. Ray, Phys. Rev. D **73**, 114007 (2006).
[20] E. Megías, E. R. Arriola, and L. L. Salcedo, Phys. Rev. D **74**, 065005 (2006).
[21] C. Ratti, M. A. Thaler, and W. Weise, Phys. Rev. D **73**, 014019 (2006).
[22] S. Rößner, C. Ratti, and W. Weise, Phys. Rev. D **75**, 034007 (2007).
[23] K. Kashiwa, H. Kouno, M. Matsuzaki, and M. Yahiro, Phys. Lett. B **662**, 26 (2008).
[24] Y. Sakai, K. Kashiwa, H. Kouno, and M. Yahiro, Phys. Rev. D **77**, 051901(R) (2008).
[25] Y. Sakai, K. Kashiwa, H. Kouno, and M. Yahiro, Phys. Rev. D **78**, 036001 (2008).
[26] Y. Sakai, K. Kashiwa, H. Kouno, M. Matsuzaki, and M. Yahiro, Phys. Rev. D **78**, 076007 (2008).
[27] Y. Sakai, K. Kashiwa, H. Kouno, M. Matsuzaki, and M. Yahiro, Phys. Rev. D **79**, 096001 (2009).
[28] Y. Sakai, H. Kouno, and M. Yahiro, J. Phys. G **37**, 105007 (2010).
[29] P. Cea, L. Cosmai, M. D'Elia, C. Manneschi, and A. Papa, Phys. Rev. D **80**, 034501 (2009).
[30] C. Bonati, M. D'Elia, M. Mariti, M. Mesiti, F. Negro, and F. Sanfilippo, Phys. Rev. D **90**, 114025 (2014).
[31] C. Bonati, M. D'Elia, M. Mariti, M. Mesiti, F. Negro, and F. Sanfilippo, Phys. Rev. D **92**, 054503 (2015).
[32] C. Bonati, M. D'Elia, M. Mariti, M. Mesiti, F. Negro, and F. Sanfilippo, Phys. Rev. D **93**, 074504 (2016).
[33] M. D'Elia, G. Gagliardi, and F. Sanfilippo, Phys. Rev. D **95**, 094503 (2017).
[34] G. Boyd, J. Engels, F. Karsch, E. Laermann, C. Legeland, M. Lütgemeire, and B. Petersson, Nucl. Phys. **B469**, 419 (1996).
[35] O. Kaczmarek, F. Karsch, P. Petreczky, and F. Zantow, Phys. Lett. B **543**, 41 (2002).
[36] E. Laermann and O. Philipsen, Annu. Rev. Nucl. Part. Sci. **53**, 163 (2003).
[37] Z. Fodor and S. D. Katz, arXiv:0908.3341.
[38] S. Borsányi, Z. Fodor, C. Hoelbling, S. D. Katz, S. Krieg, C. Ratti, and K. K. Szabo, J. High Energy Phys. 09 (2010) 073.
[39] W. Söldner, Proc. Sci., LATTICE2010 (**2010**) 215.
[40] K. Kanaya, AIP Conf. Proc. **1343**, 57 (2011); arXiv: 1012.4247.
[41] T. Sasaki, Y. Sakai, H. Kouno, and M. Yahiro, Phys. Rev. D **84**, 091901(R) (2011).
[42] G. 't Hooft, Phys. Rev. Lett. **37**, 8 (1976); Phys. Rev. D **14**, 3432 (1976).
[43] M. Kobayashi and T. Maskawa, Prog. Theor. Phys. **44**, 1422 (1970).
[44] M. Kobayashi, H. Kondo, and T. Maskawa, Prog. Theor. Phys. **45**, 1955 (1971).
[45] P. Rehberg, S. P. Klevansky, and J. Hüfner, Phys. Rev. C **53**, 410 (1996).
[46] S. P. Klevansky, Rev. Mod. Phys. **64**, 649 (1992).
[47] H. Kouno, Y. Sakai, K. Kashiwa, and M. Yahiro, J. Phys. G **36**, 115010 (2009).
[48] C. Sasaki, B. Friman, and K. Redlich, Phys. Rev. D **75**, 074013 (2007).
[49] K. Kashiwa and A. Ohnishi, Phys. Lett. B **750**, 282 (2015); Phys. Rev. D **93**, 116002 (2016); arXiv:1701.04953.
[50] Y. Sakai, T. Sasaki, H. Kouno, and M. Yahiro, Phys. Rev. D **82**, 076003 (2010).
[51] Y. Sakai, T. Sasaki, H. Kouno, and M. Yahiro, J. Phys. G **39**, 035004 (2012).
[52] J. Sugano, J. Takahashi, M. Ishii, H. Kouno, and M. Yahiro, Phys. Rev. D **90**, 037901 (2014); J. Sugano, H. Kouno, and M. Yahiro, Phys. Rev. D **94**, 014024 (2016).
[53] S. Ejiri, Y. Maezawa, N. Ukita, S. Aoki, T. Hatsuda, N. Ishii, K. Kanaya, and T. Umeda, Phys. Rev. D **82**, 014508 (2010).
[54] N. K. Glendenning, Phys. Lett. **114B**, 392 (1982).
[55] J. Schaffner and I. N. Mishustin, Phys. Rev. C **53**, 1416 (1996).
[56] C. Ishizuka, A. Ohnishi, K. Tsubakihara, K. Sumiyoshi, and S. Yamada, J. Phys. G **35**, 085201 (2008).
[57] K. Tsubakihara, H. Maekawa, H. Matsumiya, and A. Ohnishi, Phys. Rev. C **81**, 065206 (2010); K. Tsubakihara, A. Ohnishi, and T. Harada, arXiv:1402.0979.
[58] S. Weissenborn, D. Chatterjee, and J. Schaffner-Bielich, Nucl. Phys. **A881**, 62 (2012); Phys. Rev. C **85**, 065802 (2012); Nucl. Phys. **A914**, 421 (2013).
[59] P. B. Demorest, T. Pennucci, S. M. Ransom, M. S. E. Roberts, and J. W. T. Hessels, Nature (London) **467**, 1081 (2010).
[60] J. Antoniadis *et al.*, Science **340**, 1233232 (2013).